Supplementary Materials

EMUDRA: Ensemble of Multiple Drug Repositioning Approaches to Improve Prediction Accuracy

Xianxiao Zhou[1,2], Minghui Wang[1,2], Igor Katsyv[1,2,3], Hanna Irie[4,5] and Bin Zhang[1,2,5]*

[1]Department of Genetics and Genomic Sciences, Icahn School of Medicine at Mount Sinai, New York, NY, 10029. [2]Icahn Institute for Genomics and Multiscale Biology, Icahn School of Medicine at Mount Sinai, New York, NY, 10029. [3]Medical Scientist Training Program, Icahn School of Medicine at Mount Sinai, New York, NY, 10029. [4]Division of Hematology and Medical Oncology, Department of Medicine, Icahn School of Medicine at Mount Sinai, New York, NY, 10029. [5]Department of Oncological Sciences, Tisch Cancer Institute, Icahn School of Medicine at Mount Sinai, New York, NY, 10029.

*Correspondence:

Bin Zhang, PhD.
Professor
Department of Genetics & Genomic Sciences
Icahn School of Medicine at Mount Sinai
1470 Madison Avenue, Room S8-111, New York, NY 10029
(Phone) 212-824-8947 (Fax) 646-537-8660
Email: bin.zhang@mssm.edu or zhangb@hotmail.com

Supplementary Results

Normality of Matching Scores

Application of EMUDRA to Ovarian Cancer

Availability of Additional Data and Scripts

Supplementary Tables

Table S1. Composition scores for the 247 ensemble and 8 non-ensemble methods

Table S2. The top 20 drugs for ovarian cancer predicted by EMUDRA

Supplementary Figures

Figure S1. Receiver operator characteristic (ROC) curves and partial area under the curve (pAUC) of the 9 methods in simulations.

Figure S2. ROC curves and whole AUC of the 9 methods in simulations.

Figure S3. ROC curves and partial AUC of simulations with higher noise.

Figure S4. ROC curve and partial AUC of the 9 methods in independent data sets.

Figure S5. ROC curve and whole AUC of the 9 methods in independent data sets.

Figure S6. Distributions of p-values from normality tests of random signatures and distributions of scores.

Supplementary Data

Images used to generate Figure 5B.

Supplementary Results

Normality of Matching Scores

We tested the normality of the distribution of each of 4 sets of scores from 4 non-ensemble methods composing EMUDRA. We first tested distributions of enrichment scores calculated from random signatures. Each random signature was comprised of 5,000 genes randomly sampled from all the genes profiled in CMap, while gene expression changes (logFC) were randomly generated from a uniform distribution $U[-1, 1]$. Enrichment scores from each method were then compared to a normal distribution with their mean and standard deviation using K-S test. A total of 100 random signatures were tested. As shown in Figure S6A, most of score lists calculated from the 100 random signatures followed normal distribution with p-value > 0.05. Specifically, only 1, 4, 0 and 4 of the 100 signatures showed a non-normal distribution (i.e. $p \leq 0.05$) for Cosine, XCor, XSpe and EWCos methods, respectively. These result indicated that enrichment scores of random signatures followed normal distribution (a typical example shown in Fig. S6B). Next, we tested normality of the scores calculated from the TNBC signature. As expected, those scores did not follow normal distributions as a few drugs reversed the TNBC signature, which formed long tails at the negative parts of the distributions (Fig. S6C). However, after excluding enrichment scores less than -0.06, the remaining scores followed normal distributions (Fig. S6D). These results supported our assumption that matching scores of the 4 methods would follow normal distribution except those scores from drugs that matched (reversed/enhanced) with query signature.

Application of EMUDRA to Ovarian Cancer

We further applied EMUDRA to ovarian cancer. We first identified the genes differentially expressed between the stage IV ovarian cancer samples (distant metastasis) and the stage I-III samples (without distant metastasis) in the TCGA cohort. This signature included 114 up-regulated and 109 down-regulated genes in stage IV ovarian cancer. Table S2 shows the top 20 drugs predicted by EMUDRA. Fifteen of the top 20 drugs have known anticancer effects, such as apoptosis, cell cycle arrest and suppress cancer cell growth, suggesting that the top drugs have potential effects on suppressing ovarian cancer growth, aggression and metastasis. Among these drugs, only ciclopirox is in the top 20 drugs previously identified for the triple negative breast cancer, indicating EMUDRA adapts to input signatures of interest.

Availability of Additional Data and Scripts

The data and script for making Figures 2-4 are available from the Synapse (https://www.synapse.org/#!Synapse:syn11038303).

Supplementary Tables

Table S1. Composition scores for the 247 ensemble and 8 non-ensemble methods.

Ensemble	Composite.Score	Ensemble	Composite.Score	Ensemble	Composite.Score
Cos.XCor.XSpe.EWCos (EMUDRA)	0.479638	Cos.XSum.XSpe.WSS	0.037747	XCos.XCor.EWCos.KS	5.02E-13
Cos.XCos.XCor.XSpe.EWCos.WSS	0.442958	XSum.XCos.EWCos.WSS	0.036908	XCor.XSpe.KS	5.02E-13
Cos.XCos.XSpe.EWCos	0.441615	Cos.XSum.EWCos.WSS	0.03521	XSum.XCor.EWCos.KS.WSS	4.88E-13
Cos.XSpe.EWCos	0.415415	Cos.XSum.EWCos	0.030451	Cos.XSum.XCor.XSpe.KS.WSS	4.88E-13
Cos.XCos.XCor.EWCos.WSS	0.412619	Cos.XSum.XCor	0.029668	XCor.XSpe.EWCos.KS	4.83E-13
Cos.XCor.XSpe.EWCos.WSS	0.404975	Cos.XSum.XSpe	0.025822	Cos.XCos.XCor.XSpe.KS.WSS	4.82E-13
Cos.XCos.XCor.XSpe.EWCos	0.391374	XSum.XCos.XCor.XSpe	0.025749	Cos.XCor.XSpe.EWCos.KS	4.64E-13
Cos.XCor.EWCos	0.387216	Cos.XSum.XCos	0.025223	XCos.XCor.XSpe.KS.WSS	4.56E-13
Cos.XCos.XSpe.EWCos.WSS	0.380861	XSum.XCor.EWCos	0.025127	XSum.XCor.KS.WSS	4.50E-13
Cos.XCos.XCor.EWCos	0.354182	XSum.XCos.XCor.WSS	0.023669	Cos.XSum.XCor.EWCos.KS.WSS	4.43E-13
Cos.XCor.EWCos.WSS	0.328538	XSum.XCos.EWCos	0.02301	Cos.XCor.XSpe.KS	4.40E-13
Cos.XCos.EWCos	0.305494	XSum.XCor.XSpe.WSS	0.022735	Cos.XCos.XCor.XSpe.EWCos.KS.WSS	4.39E-13
Cos.XSpe.EWCos.WSS	0.297396	XSum.XSpe.EWCos.WSS	0.022026	XCos.XCor.XSpe.EWCos.KS.WSS	4.35E-13
Cos.XSpe	0.283303	XSum.XCos.XSpe.WSS	0.020461	Cos.XSum.XCor.KS.WSS	4.29E-13
Cos.XSum.XCos.XCor.XSpe.EWCos.WSS	0.282022	XCos.XCor	0.019251	Cos.XSum.XSpe.EWCos.KS	4.05E-13
Cos.XCos.EWCos.WSS	0.280198	XSum.XSpe.EWCos	0.015053	XSum.XCos.XSpe.EWCos.KS.WSS	4.00E-13
XCos.XCor.XSpe.EWCos.WSS	0.258072	XSum.XCor.XSpe	0.014159	Cos.XSum.XCos.XSpe.EWCos.KS.WSS	3.86E-13
Cos.XSum.XCor.XSpe.EWCos.WSS	0.255655	XSum.XCos.XCor	0.013057	XSum.XSpe.EWCos.KS	3.79E-13
Cos.XCor.XSpe.WSS	0.253148	XSum.XCos.XSpe	0.01252	XSum.XCos.EWCos.KS.WSS	3.54E-13
Cos.XCos.XCor.XSpe.WSS	0.243792	XCor.WSS	0.011603	Cos.XSum.XCos.XSpe.KS.WSS	3.40E-13
Cos.XSum.XCos.XCor.EWCos.WSS	0.242628	XCos.WSS	0.010951	XSum.XCos.XSpe.KS.WSS	3.34E-13
XCor.XSpe.EWCos.WSS	0.241665	XSum.XCor.WSS	0.009483	XSum.EWCos.KS	3.28E-13
Cos.XSum.XCos.XSpe.EWCos.WSS	0.235064	Cos.WSS	0.007194	Cos.XSum.XCos.EWCos.KS.WSS	3.25E-13
Cos.XCor.XSpe	0.234406	XSum.XCos.WSS	0.006663	XCos.XCor.EWCos.KS.WSS	3.20E-13
XCor.XSpe.EWCos	0.228843	XSum.XCor	0.005727	XCos.XSpe.KS	3.13E-13
XCos.XSpe.EWCos	0.227075	XSpe.WSS	0.005663	Cos.XCos.XCor.EWCos.KS.WSS	3.12E-13
XCos.XSpe.EWCos.WSS	0.2241	XSum.XCos	0.004724	Cos.XCos.XSpe.EWCos.KS	3.08E-13
Cos.XCos.XSpe.WSS	0.223103	Cos.XSum.WSS	0.004572	Cos.XSum.EWCos.KS	3.08E-13
Cos.XCor	0.208147	Cos.XSum	0.003908	Cos.XCos.XSpe.KS	3.06E-13
Cos.XSum.XCos.XCor.XSpe.EWCos	0.205838	XSum.XSpe.WSS	0.002768	XCos.XSpe.EWCos.KS	2.97E-13
XCos.XCor.EWCos.WSS	0.20539	XSum.XSpe	0.002243	XSum.XCos.KS.WSS	2.97E-13
Cos.XCos.XSpe	0.202481	XSum.EWCos.WSS	0.002128	Cos.XSum.XSpe.KS	2.96E-13
XSpe.EWCos	0.199096	XSum.EWCos	0.001514	Cos.XSum.XCos.KS.WSS	2.89E-13
Cos.XSum.XCor.XSpe.EWCos	0.19072	EWCos.WSS	0.000575	Cos.XCos.XCor.KS.WSS	2.78E-13
Cos.XCos.XCor.WSS	0.187936	XSum.WSS	0.00039	XCos.XCor.KS.WSS	2.70E-13
Cos.XSum.XCor.EWCos.WSS	0.181113	XSpe	4.62E-05	Cos.XCor.KS	2.60E-13
XCos.XCor.XSpe.EWCos	0.178179	XCor	4.30E-05	XCor.EWCos.KS	2.55E-13
Cos.XSum.XCos.XSpe.EWCos	0.174028	Cosine	1.63E-05	Cos.XCor.EWCos.KS	2.52E-13
Cos.XSum.XCos.XCor.EWCos	0.168451	XCos	5.02E-06	XCor.KS	2.45E-13
Cos.XSum.XCos.EWCos.WSS	0.165931	EWCos	2.34E-06	XSum.XSpe.EWCos.KS.WSS	2.45E-13
Cos.XCos	0.159098	XSum	3.63E-07	Cos.XSum.XSpe.EWCos.KS.WSS	2.39E-13
XCor.EWCos	0.156394	KS	3.46E-07	Cos.XSum.KS	2.31E-13
Cos.XSum.XSpe.EWCos.WSS	0.149852	WSS	2.86E-07	XSum.XSpe.KS	2.22E-13
Cos.XCos.XCor.XSpe	0.148278	XSum.XCos.XCor.XSpe.KS	1.14E-12	Cos.XSum.XSpe.KS.WSS	1.88E-13
Cos.XCor.WSS	0.136663	XSum.XCos.XCor.KS	1.10E-12	Cos.XSum.EWCos.KS.WSS	1.81E-13
Cos.XSum.XCor.EWCos	0.131166	Cos.XSum.XCos.XCor.XSpe.KS	1.09E-12	Cos.XCor.XSpe.KS.WSS	1.81E-13
XSum.XCos.XCor.XSpe.EWCos.WSS	0.129586	XSum.XCos.XCor.XSpe.EWCos.KS	1.08E-12	Cos.XCor.XSpe.EWCos.KS.WSS	1.67E-13
Cos.XSum.XCos.XCor.XSpe.WSS	0.129351	Cos.XSum.XCos.XCor.KS	1.04E-12	Cos.XCos.EWCos.KS	1.59E-13
XCos.XCor.EWCos	0.124327	XSum.XCos.XCor.EWCos.KS	1.03E-12	XSum.XSpe.KS.WSS	1.55E-13
XCos.EWCos	0.120184	Cos.XSum.XCos.XCor.XSpe.EWCos.KS	9.92E-13	XSum.EWCos.KS.WSS	1.55E-13
Cos.XSum.XSpe.EWCos	0.119321	Cos.XSum.XCos.XCor.EWCos.KS	9.66E-13	Cos.XCos.KS	1.49E-13
Cos.XSum.XCos.EWCos	0.110398	XSum.XCor.XSpe.EWCos.KS	9.28E-13	XCor.XSpe.EWCos.KS.WSS	1.47E-13
Cos.XCos.XCor	0.11011	XSum.XCos.XCor.XSpe.KS.WSS	8.76E-13	XSum.KS	1.42E-13
Cos.XCos.WSS	0.107638	Cos.XSum.XCor.XSpe.EWCos.KS	8.55E-13	XCos.EWCos.KS	1.34E-13
Cos.XSpe.WSS	0.101884	XSum.XCor.XSpe.KS	8.40E-13	Cos.XCos.XSpe.EWCos.KS.WSS	1.32E-13
XCor.EWCos.WSS	0.101805	Cos.XSum.XCor.XSpe.KS	8.33E-13	XCor.XSpe.KS.WSS	1.31E-13
Cos.XSum.XCor.XSpe.WSS	0.097483	XSum.XCor.EWCos.KS	8.26E-13	Cos.XSum.KS.WSS	1.30E-13
XSum.XCor.XSpe.EWCos.WSS	0.094811	XSum.XCos.XCor.XSpe.EWCos.KS.WSS	7.73E-13	Cos.XCos.XSpe.KS.WSS	1.12E-13
Cos.XSum.XCos.XSpe.WSS	0.089156	Cos.XSum.XCor.EWCos.KS	7.52E-13	XCos.XSpe.EWCos.KS.WSS	1.01E-13
XSum.XCos.XCor.EWCos.WSS	0.088869	Cos.XSum.XCor.KS	7.50E-13	XSum.KS.WSS	9.50E-14
Cos.XSum.XCos.XCor.WSS	0.087933	XCos.XCor.XSpe.KS	7.49E-13	XCos.KS	9.22E-14
Cos.EWCos	0.086141	Cos.XSum.XCos.XCor.XSpe.KS.WSS	7.36E-13	Cos.XCor.EWCos.KS.WSS	8.95E-14
XCos.EWCos.WSS	0.085832	XSum.XCos.XCor.KS.WSS	7.31E-13	XCos.XSpe.KS.WSS	8.03E-14
XSum.XCos.XSpe.EWCos.WSS	0.085405	XSum.XCos.XSpe.EWCos.KS	7.17E-13	Cos.XCor.KS.WSS	7.05E-14
XSpe.EWCos.WSS	0.084821	XSum.XCos.XCor.EWCos.KS.WSS	7.13E-13	Cos.XSpe.EWCos.KS	6.72E-14

Table S1. Composition scores for the 247 ensemble and 8 non-ensemble methods. (Continued)

Ensemble	Composite.Score	Ensemble	Composite.Score	Ensemble	Composite.Score
XSum.XCos.XCor.XSpe.EWCos	0.083244	CombnAll8Scores	7.08E-13	XCor.EWCos.KS.WSS	6.11E-14
XCos.XCor.XSpe.WSS	0.079339	XSum.XCor.KS	6.92E-13	Cos.XCos.EWCos.KS.WSS	5.75E-14
Cos.XSum.XCos.XCor.XSpe	0.078543	Cos.XSum.XCos.XSpe.EWCos.KS	6.77E-13	Cos.XCos.KS.WSS	4.13E-14
Cos.XSum.XCor.XSpe	0.057925	Cos.XCos.XCor.XSpe.KS	6.41E-13	XSpe.EWCos.KS	3.98E-14
XSum.XCor.XSpe.EWCos	0.057257	XCos.XCor.KS	6.33E-13	Cos.XSpe.KS	3.96E-14
Cos.XSum.XCos.XSpe	0.052562	XSum.XCos.XSpe.KS	6.24E-13	XCos.EWCos.KS.WSS	3.59E-14
XSum.XCos.XSpe.EWCos	0.051643	XCos.XCor.XSpe.EWCos.KS	6.19E-13	XCor.KS.WSS	3.36E-14
Cos.XSum.XCor.WSS	0.051379	Cos.XSum.XCos.XCor.EWCos.KS.WSS	6.18E-13	Cos.XSpe.EWCos.KS.WSS	2.85E-14
XSum.XCos.XCor.EWCos	0.051273	Cos.XSum.XCos.XSpe.KS	6.18E-13	XCos.KS.WSS	2.12E-14
Cos.XSum.XCos.XCor	0.051069	Cos.XSum.XCos.XCor.KS.WSS	6.13E-13	Cos.EWCos.KS	1.91E-14
XCor.XSpe.WSS	0.050402	Cos.XCos.XCor.XSpe.EWCos.KS	6.11E-13	Cos.XSpe.KS.WSS	1.89E-14
Cos.EWCos.WSS	0.048199	XSum.XCos.EWCos.KS	6.06E-13	XSpe.EWCos.KS.WSS	1.70E-14
XCos.XSpe.WSS	0.047699	Cos.XSum.XCos.EWCos.KS	5.76E-13	XSpe.KS	1.57E-14
Cos.XSum.XCos.WSS	0.044673	Cos.XSum.XCos.KS	5.51E-13	Cos.EWCos.KS.WSS	1.15E-14
XCos.XSpe	0.044441	XSum.XCor.XSpe.EWCos.KS.WSS	5.44E-13	XSpe.KS.WSS	1.04E-14
XSum.XCor.EWCos.WSS	0.043522	XSum.XCos.KS	5.29E-13	Cos.KS	7.66E-15
XSum.XCos.XCor.XSpe.WSS	0.042927	Cos.XCos.XCor.KS	5.23E-13	EWCos.KS	5.84E-15
XCor.XSpe	0.041818	Cos.XCos.XCor.EWCos.KS	5.18E-13	Cos.KS.WSS	5.66E-15
XCos.XCor.WSS	0.038536	XSum.XCor.XSpe.KS.WSS	5.13E-13	EWCos.KS.WSS	4.13E-15
XCos.XCor.XSpe	0.038147	Cos.XSum.XCor.XSpe.EWCos.KS.WSS	5.13E-13	KS.WSS	1.24E-15

Table S2. Top 20 drugs targeting ovarian cancer by EMUDRA

Drug	Score	Known Effects	Evidence type	Reference
ciclopirox	-6.74303	Inhibit cell proliferation	direct	(Shen, et al., 2017)
gossypol	-6.33088	Induce apoptosis	indirect	(Volate, et al., 2010)
perhexiline	-6.30989	Inhibit tumor growth	direct	(Ren, et al., 2015)
monensin	-6.29086	Cell cycle arrest and apoptosis	direct	(Park, et al., 2003)
5182598	-6.08998	Novel prediction	unclear	None
phenoxybenzamine	-5.70601	Novel prediction	unclear	None
MG-132	-5.67589	Induce autophagy	indirect	(Bao, et al., 2016)
clofilium tosylate	-5.62421	Induce apoptosis with pazopanib	direct	(Chauvin, et al., 2017)
pararosaniline	-5.5809	Novel prediction	unclear	None
thioridazine	-5.26889	Induce apoptosis	indirect	(Kang, et al., 2012)
clomipramine	-5.14264	Induce apoptosis	indirect	(Xia, et al., 1999)
rescinnamine	-5.10425	Induce apoptosis	indirect	(AbdelHafez, et al., 2013)
dyclonine	-5.06724	Enhance cytotoxic effect	indirect	(Ju, et al., 2009)
pimethixene	-4.832	Novel prediction	unclear	None
clofazimine	-4.77852	Inhibit cancer cell growth	direct	(Koval, et al., 2014)
niclosamide	-4.76828	Suppress cancer cell growth	direct	(Lu, et al., 2011)
triamterene	-4.72708	Selective tumor cell cytotoxicity	direct	(Guillotin, et al., 2017)
withaferin A	-4.71359	Kills cancer cells	direct	(Yu, et al., 2017)
clioquinol	-4.5358	Reduced cancer cell viability	direct	(Ding, et al., 2005)
5151277	-4.5082	Novel prediction	unclear	None

Supplementary Figures

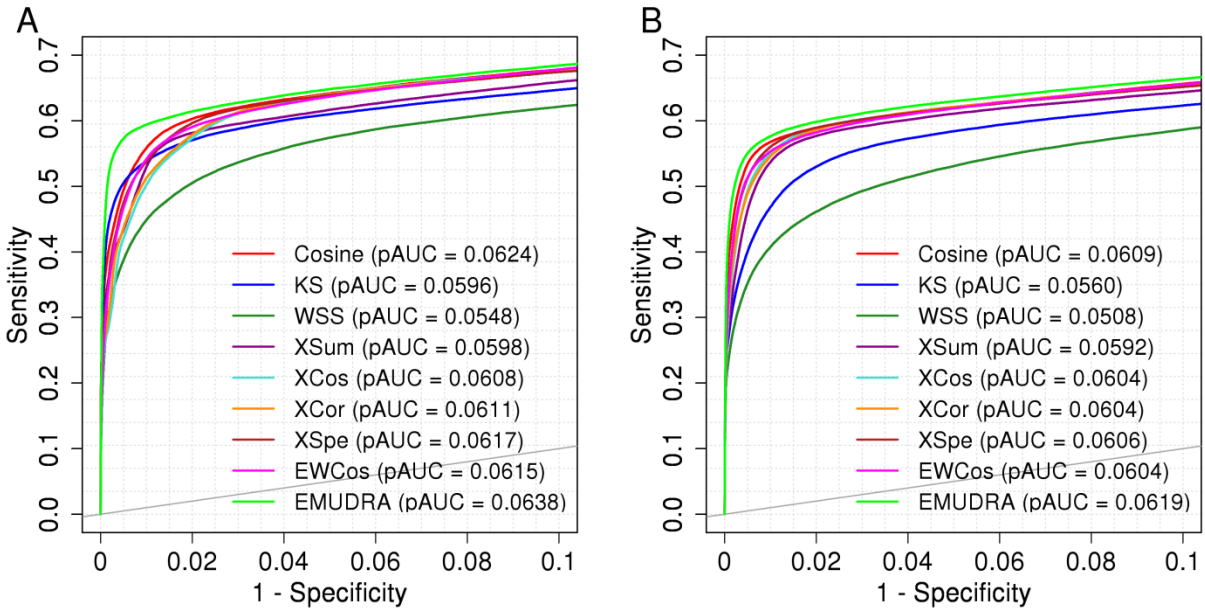

Figure S1. Receiver operator characteristic (ROC) curves and partial area under the curve (pAUC) of the 9 methods in the simulation studies. (A) Drug-induced signatures were identified from drug-treated and vehicle-treated gene expression profiles for each instance in the CMap. Those signatures were used as query signatures to calculate scores for each method. Instances treated with a same drug of a query signature were taken as positive cases while the other instances were set as negative cases for plotting ROC curves and assessing AUC of false positive rate less than 0.1. **(B)** Partial ROC and AUC of signatures identified from the CMap gene expression profiles with adding random noise from a uniform distribution.

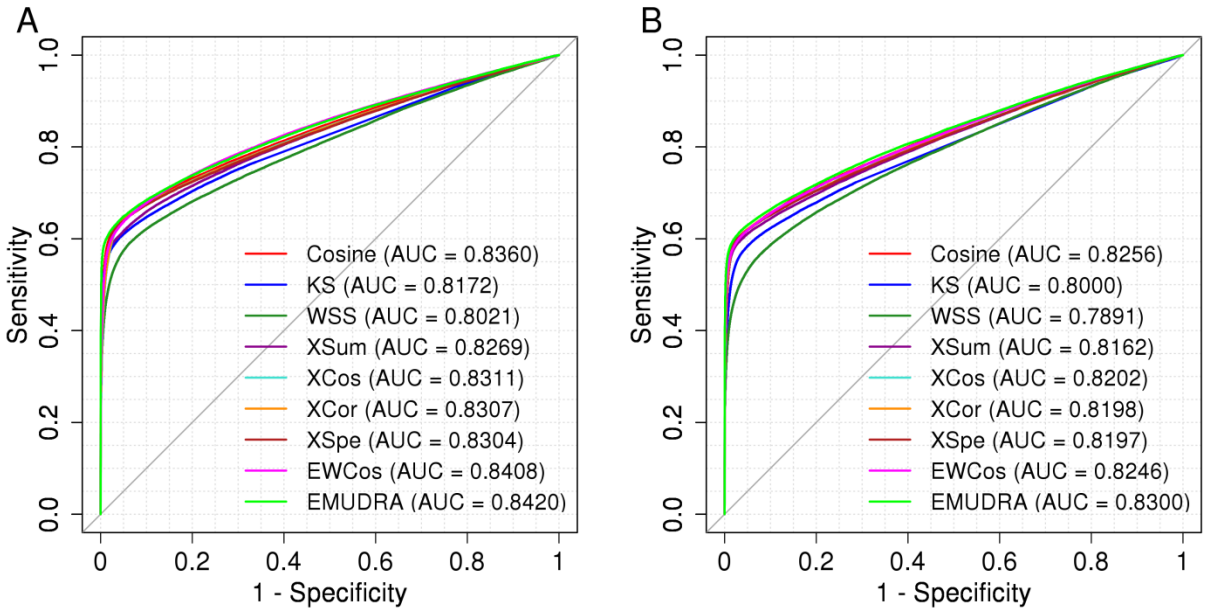

Figure S2. ROC curves and whole AUC of the 9 methods in simulations. (A) Drug-induced signatures were identified from drug-treated and vehicle-treated gene expression profiles for each instance in the CMap. Those signatures were used as query signatures to calculate scores for each method. Instances treated with a same drug of a query signature were set as positive cases and other instances were set as negative cases for plotting ROC curves and assessing the AUC. **(B)** ROC and AUC of signatures identified from the CMap gene expression profiles with adding random noise from a uniform distribution.

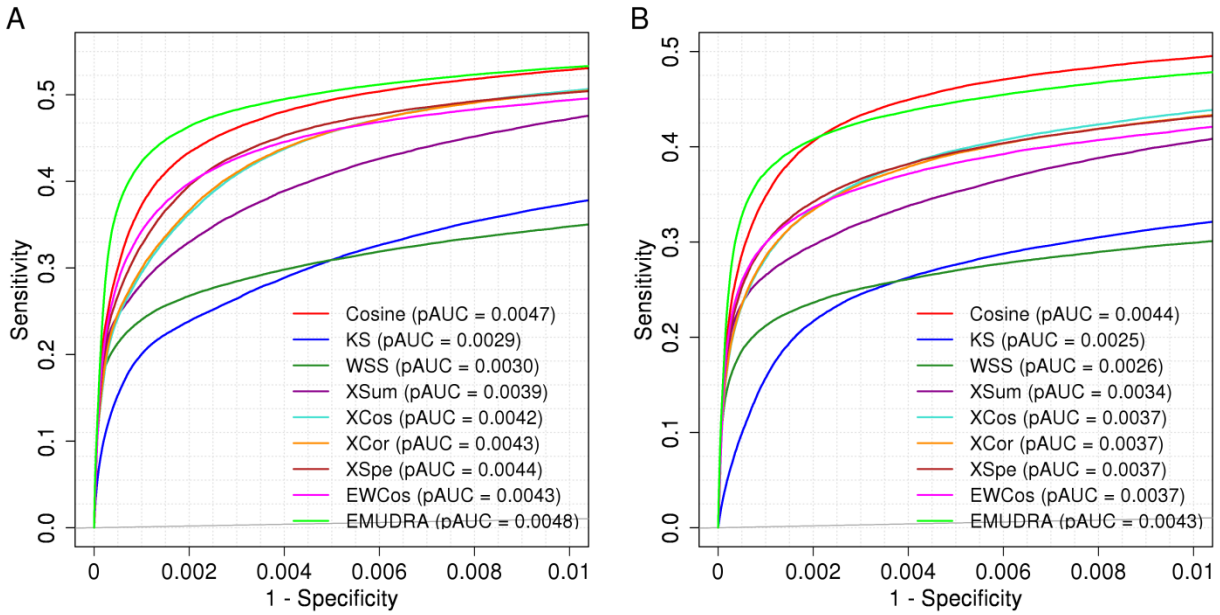

Figure S3. ROC curves and partial AUC of simulations with higher noise. (A) Random noise (s = 0.5) from a uniform distribution was added to the CMap gene expression profiles to identify query signatures. Those signatures were used as query signatures to calculate scores for each method. Instances treated with a same drug of a query signature were set as positive cases and other instances were set as negative cases for plotting ROC curves and assessing partial AUC of false positive rate less than 0.01. (B) pROC and pAUC of s = 0.8

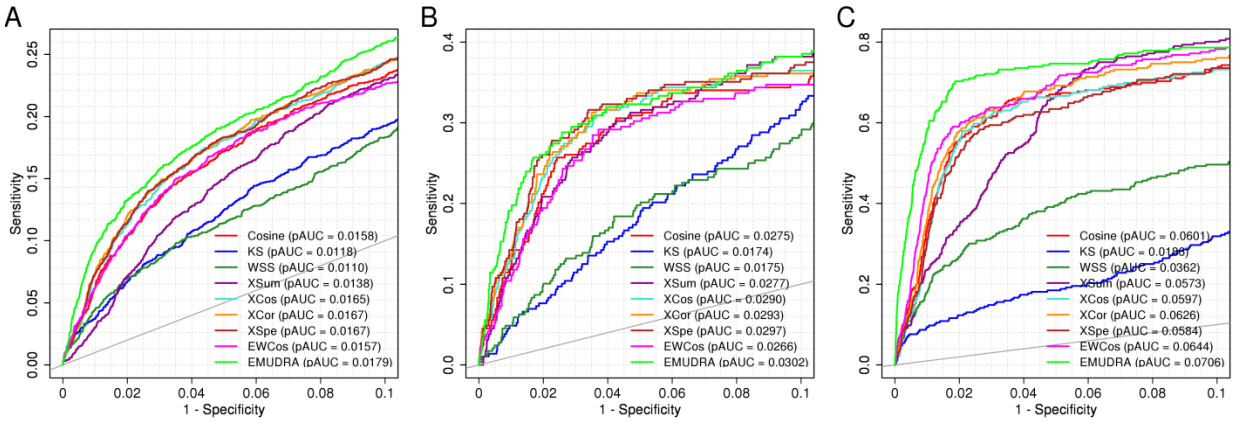

Figure S4. ROC curve and partial AUC of the 9 methods in independent data sets. (A) ROC curves and pAUC of predicting drug pairs sharing at least 1 ATC code. Drug pairs sharing at least 1 ATC level 4 codes were used as positive cases and other drug pairs between those drugs were set as negative cases. Drug-induced signatures identified from the CMap were used as query signatures to calculate scores of drug pairs for each method. The positive and negative cases as well as scores were then used to generate ROC curves and evaluate pAUC of the 9 methods with FPR less than 0.1. (B) Predicting drug pairs sharing at least 2 ATC codes. (C) ROC curves and pAUC of the LINCS validation data set. Drug-induced signatures were identified from the LINCS data set and used to calculate scores. Instances treated with the same drug of a signature were used as positive cases and other instances were used as negative cases to generate ROC curves and calculate pAUC with FPR less than 0.1.

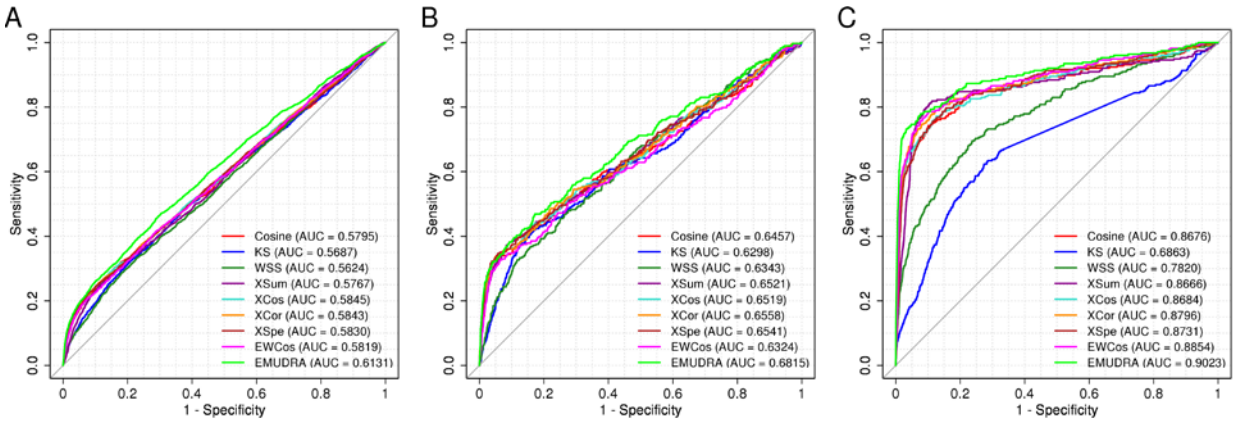

Figure S5. ROC curves and whole AUC of 9 methods tested in the independent data sets. (A) ROC curves and AUC of predicting drug pairs sharing at least 1 ATC code. Drug pairs sharing at least 1 ATC level 4 codes were used as positive cases and other drug pairs among those drugs were set as negative cases. Drug-induced signatures identified from CMap were used as query signatures to calculate matching scores of drug pairs using each method. The positive and negative cases as well as scores were then used to generate ROC curves and estimate AUC. (B) Predicting drug pairs sharing at least 2 ATC codes. (C) ROC curves and AUC of the LINCS validation data set. Drug-induced signatures were identified from the LINCS data set and used to calculate scores. Instances treated with the same drug of a signature were used as positive cases and other instances were used as negative cases to generate ROC curves and calculate AUC.

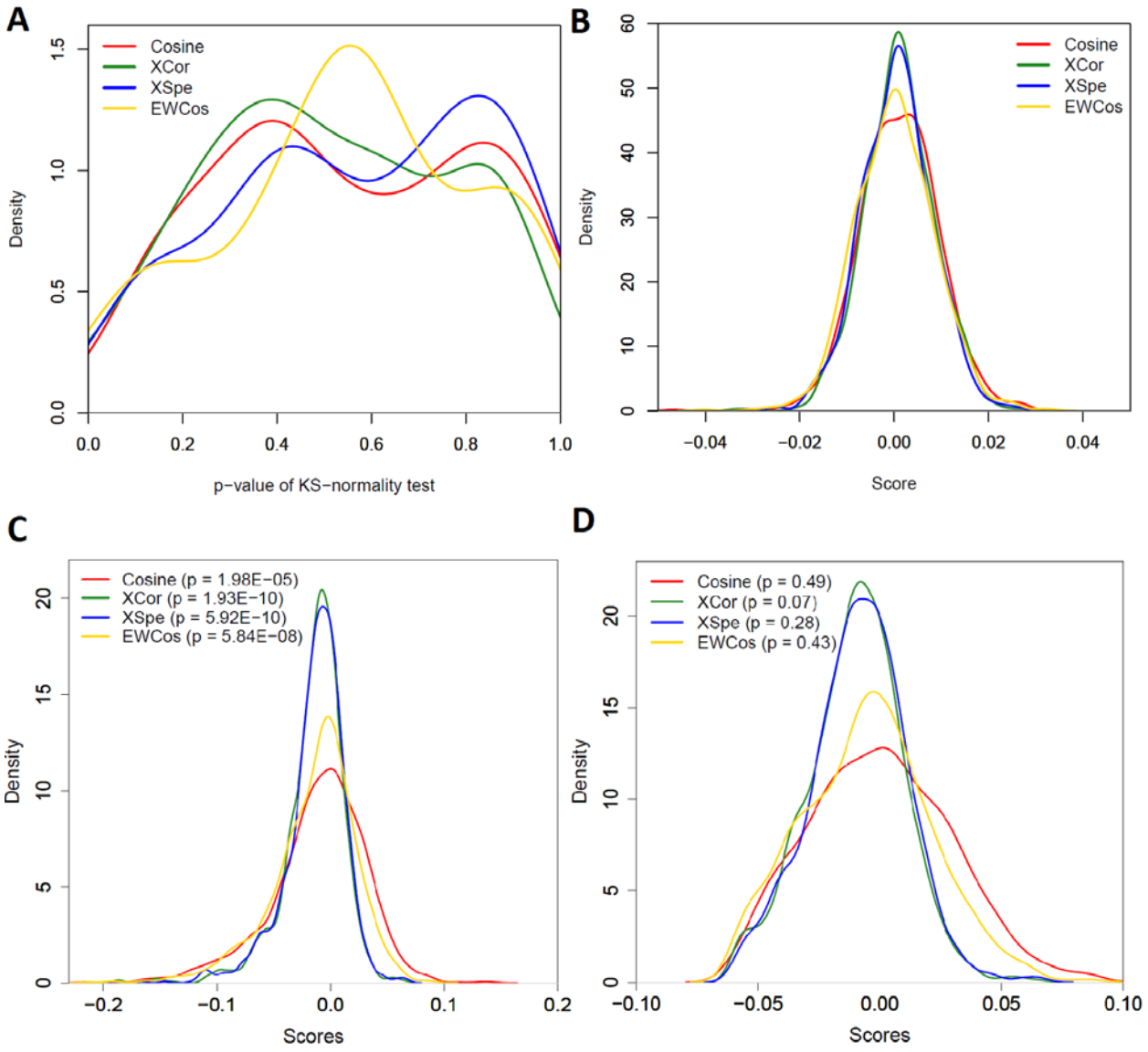

Figure S6. Distributions of p-values from normality tests of random signatures and distributions of matching scores from the four methods composing EMUDRA. (A) Distributions of p-values from normality tests of Cosine, XCor, XSpe and EWCos scores calculated from random signatures. (B) Distributions of Cosine, XCor, XSpe and EWCos scores from a random signature. (C) Distributions of Cosine, XCor, XSpe and EWCos scores from the triple negative breast cancer signature. The p-values were calculated by comparing scores of each method with standard normal distribution using the K-S test. (D) Distributions of Cosine, XCor, XSpe and EWCos scores from the triple negative breast cancer signature without scores < -0.06. The p-values were calculated by comparing scores of each method with standard normal distribution using the K-S test.

Reference

AbdelHafez, E.M.*, et al.* Computational and synthetic studies towards improving rescinnamine as an inducer of MSH2-dependent apoptosis in cancer treatment. *Mol Cancer Biol* 2013;1(1).

Bao, W.*, et al.* Induction of autophagy by the MG132 proteasome inhibitor is associated with endoplasmic reticulum stress in MCF7 cells. *Mol Med Rep* 2016;13(1):796-804.

Chauvin, C.*, et al.* High-Throughput Drug Screening Identifies Pazopanib and Clofilium Tosylate as Promising Treatments for Malignant Rhabdoid Tumors. *Cell Rep* 2017;21(7):1737-1745.

Ding, W.Q.*, et al.* Anticancer activity of the antibiotic clioquinol. *Cancer Res* 2005;65(8):3389-3395.

Guillotin, D.*, et al.* Drug-Repositioning Screens Identify Triamterene as a Selective Drug for the Treatment of DNA Mismatch Repair Deficient Cells. *Clin Cancer Res* 2017;23(11):2880-2890.

Ju, D., Wang, X. and Xie, Y. Dyclonine and alverine citrate enhance the cytotoxic effects of proteasome inhibitor MG132 on breast cancer cells. *Int J Mol Med* 2009;23(2):205-209.

Kang, S.*, et al.* Thioridazine induces apoptosis by targeting the PI3K/Akt/mTOR pathway in cervical and endometrial cancer cells. *Apoptosis* 2012;17(9):989-997.

Koval, A.V.*, et al.* Anti-leprosy drug clofazimine inhibits growth of triple-negative breast cancer cells via inhibition of canonical Wnt signaling. *Biochem Pharmacol* 2014;87(4):571-578.

Lu, W.*, et al.* Niclosamide suppresses cancer cell growth by inducing Wnt co-receptor LRP6 degradation and inhibiting the Wnt/beta-catenin pathway. *PLoS One* 2011;6(12):e29290.

Park, W.H.*, et al.* Monensin-mediated growth inhibition of SNU-C1 colon cancer cells via cell cycle arrest and apoptosis. *Int J Oncol* 2003;22(2):377-382.

Ren, X.R.*, et al.* Perhexiline promotes HER3 ablation through receptor internalization and inhibits tumor growth. *Breast Cancer Res* 2015;17:20.

Shen, T.*, et al.* Ciclopirox inhibits cancer cell proliferation by suppression of Cdc25A. *Genes Cancer* 2017;8(3-4):505-516.

Volate, S.R.*, et al.* Gossypol induces apoptosis by activating p53 in prostate cancer cells and prostate tumor-initiating cells. *Mol Cancer Ther* 2010;9(2):461-470.

Xia, Z.*, et al.* The antidepressants imipramine, clomipramine, and citalopram induce apoptosis in human acute myeloid leukemia HL-60 cells via caspase-3 activation. *J Biochem Mol Toxicol* 1999;13(6):338-347.

Yu, Y.*, et al.* Withaferin-A kills cancer cells with and without telomerase: chemical, computational and experimental evidences. *Cell Death Dis* 2017;8(4):e2755.